Volume 1 | Number 1 | Jan 2013 | Pages 1–100

Journal of
Materials Chemistry A

Materials for energy and sustainability
www.rsc.org/materialsA

ROYAL SOCIETY
OF CHEMISTRY

ROYAL SOCIETY
OF CHEMISTRY

www.rsc.org/materialsA

Journal of Materials Chemistry A

ARTICLE

Designed Synthesis of Sulfonated Polystyrene/Mesoporous Silica Hollow Nanospheres as Efficient Solid Acid Catalysts

Xiaomin Zhang [a,b], Lei Zhang [a] and Qihua Yang*[a]

We report the successful synthesis of hybrid hollow nanospheres (HNs) with sulfonated polystyrene ($PS-SO_3H$) aligned uniformly in the mesoporous channel of silica shell. The fabrication process involved the sulfonation of silica HNs with polystyrene highly dispersed in the mesoporous shell which were prepared by co-condensation of mixture of tetraethoxysilane (TEOS) and alkoxysilyl-functionalized poly(methyl acrylate) (PMA) around PS nanospheres in base medium using cetyltrimethylammonium bromide (CTAB) as structural directing agent followed by THF treatment. The surface properties of the hybrid HNs were adjusted by the amout of PMA incorporated in the silica shell during the synthesis process and also by modification with octyl group through grafting method. The hybrid HNs with acid exchange capacity in the range of of 0.8 to 2.0 mmolg^{-1} could efficiently catalyze esterification reaction of lauric with ethanol. All hybrid HNs show much higher activity than commercial Amberlyst®-15 catalyst and the TOF of the optimized hybrid HNs is almost the same as the concentrated sulfuric acid. The high activity of the hybrid HNs is mainly attributed to the uniform distribution of $PS-SO_3H$ group in the mesoporous silica shell, the penetrating mesopore and surface hydrophobicity. It was found that the recycle stability of hybrid HNs could be enhanced greatly by octyl group modification, which may prevent the leaching of $PS-SO_3H$ during the catalytic process.

Introduction

The replacement of conventional mineral liquid acids by solid acids for green chemistry has been intensively investigated because of the environmental consideration and safety concerns[1-6]. In the past years, various types of solid acid catalysts have been developed including zeolites[7-9], sulfated metal oxides[10-12] and polymer based resins[13, 14] etc. Among these solid acid catalysts, commercially available sulfonated ion-exchange resins (IERs) represented by Amberlyst ® -15 with acidic exchange capacity as high as 4.7 mmolg^{-1}, are widely used in a wide range of acid-catalyzed liquid phase reactions. However, the IERs do not exhibit high activity because most of the acidic sites buried within the polymer beads are inaccessible in many reactions due to their low surface areas and lack of porosity[15-18]. Recently, Xiao and co-workers have successfully synthesized mesoporous polymer based solid acids which showed superior catalytic activities in esterification and acylation reactions due to the high surface areas, abundant mesoporosity and high concentration of sulfonic acid groups[4, 5]. Thus, increasing the surface area and

pore volume is of extreme importance for improving the catalytic performance of IERs.

Owing to their outstanding properties, such as high surface areas, large pore volumes, tunable pores sizes and variable morphologies, mesoporous silicas have attracted much research interest and activity since their discovery[19-27]. Recently, different kinds of polymer/mesoporous silicas have been synthesized due to the combined advantages from both the polymers with versatile functional groups and mesoporous silicas with high thermal stability, ordered porous structure and high surface area[28-32]. The general strategies to incorporate polymer building blocks into mesoporous silicas involve in situ polymerization in the channels of mesoporous silicas[32, 33], post grafting approach[31], construction of mesoporous silicas in the presence of polymers[34] and so on. Usually, it is difficult to fabricate polymer/mesoporous silicas with high polymer content by these methods for avoiding the mesostructure damage or pore blocking and because of the lack of effective interactions between polymer and silica to prevent the leakage of polymers. Furthermore, most of the polymer/silica hybrid

materials do not have well defined morphology which could not guarantee high accessibility of the active sites, fast diffusion of the reactants and the products.

The previous studies show that the morphology of the solid catalysts greatly affects their catalytic performance because of the influence of the morphology on the diffusion length of the reactants and products, the exposure degree of active sites, the crystalline phase and so on. Recently, the solid catalysts with morphology of hollow nanosphere (HNs) have attracted much attention because the shortened diffusion lengths cannot only increase the reaction rates but also can improve the selectivity by decreasing the possibility for side reactions, especially for the deep reactions of the unstable products[26, 35-40]. Recently, our group found that silica hollow nanospheres with chiral functional groups and SO_3H/Pd incorporated in the shell of HNs are efficient solid catalysts for asymmetric reactions and one-pot synthesis of methyl isobutyl ketone from acetone, respectively[36, 38]. Zeng and co-workers reported that $H_4SiMo_{12}O_{40}$ functionalized silica HNs exhibited excellent catalytic activity toward benzylation of toluene[40]. However, the usage of the hollow nanospheres as catalysts is still in its infancy.

Recently, we found that the dissolved polymer could be retained in the mesoporous silica shell functionalized with polymer fragments during the synthesis of silica HNs using polymer nanospheres as hard templateres[41]. Based on this finding, herein, we reported the fabrication of efficient solid acid catalysts, $PS-SO_3H/PMA-SiO_2$ HNs (PS: polystyrene; PAM: poly(methyl acrylate)) with high content of polymers (66.4 wt.%) aligned uniformly in the mesoporous silica shell through sulfonation of $PS/PMA-SiO_2$ HNs which were synthesized by diffusion of PS core into the mesoporous silica shell functionalized with PMA fragments. The catalytic performance of hybrid solid acids were tested in the esterification of fatty acid with ethanol and the relation of polymer content and surface modification with the catalytic performance was investigated.

Experimental section

Chemicals and Reagents

All materials were of analytical grade and used as received without any further purification except of styrene. Styrene was washed through an inhibitor remover column for removing inhibitor and then distilled under vacuum before use. Cetyltrimethylammonium bromide (CTAB) and [3-(Methacryloxy) propyl]-trimethoxysilane (3-MOP, 98%) were purchased from Sigma-Aldrich Company Ltd. (USA). Tetraethoxysilane (TEOS) was obtained from Nanjing Shuguang Chemical Group (China). Methyl methacrylate (MMA, 98%), potassium persulfate ($K_2S_2O_8$), azobisisbutyronitrile (AIBN), tetrahydrofuran (THF), ethylether and other reagents were purchased from Shanghai Chemical Reagent, Inc. of the Chinese Medicine Group. Poly(methacrylate)-organosilane (PMA-Si) was synthesized by free radical polymerization of [3-(methacryloxy)propyl]-

trimethoxysilane (3-MOP) and methacrylate monomer (MA), initiated by AIBN, according to our previous report[41, 42]. The PS template spheres were prepared by emulsion polymerization in water system according to a modified method[43].

Synthetic procedures

SYNTHESIS OF PS/nPMA-SIO$_2$ HNS AND PS/SIO$_2$ HNS

PS/nPMA-SiO$_2$ HNs were synthesized under basic conditions using CTAB as surfactant micellar templates and PS nanospheres as co-templates of hollow nanospheres, PMA-Si and TEOS as precursors. In a typical synthesis, 0.20 g of CTAB was dissolved in a mixed solvent prepared from 60 mL of deionized water and 20 mL of ethanol at 50 °C under stirring for 30 minutes. After that, desired amount (0.1 to 0.20 g) of PS nanospheres dispersed in 2 mL of deionized water by sonication for 30 minutes were added to the above mixture and the mixture were stirred at 50 °C for another 30 minutes, followed by the addition of 0.7 mL of ammonium hydroxide solution (25%). 0.625 g of TEOS in 2 mL of ethanol was mixed with 0.50 g of PMA-Si in 2 mL of THF. Ten minutes later, the mixture was added dropwise under stirring. After stirring for 2 hours at 50 °C, the mixture was transferred into a Teflon-lined autoclave and aged at 100 °C under static conditions for 36 hours. The solid product was recovered by filtration and washed with water and ethanol and then dried at 60 °C overnight. After surfactant extraction in ethanol-HCl (0.75 wt. % of HCl), PS/nPMA-SiO$_2$ core shell nanospheres (CSNs) were obtained. Then the solid product (1 g) was dispersed in 200 mL of THF and the mixture was heated at 60 °C for 12 hours. After centrifugation and washing with ethanol, PS/nPMA-SiO$_2$ HNs were obtained, where n (n= 2.5, 3.3, and 5) denotes the weight ratio of PMA-Si to PS used in the synthesis process.

In a controlled experiment, PS/SiO$_2$ HNs were synthesized in a similar method to PS/5PMA-SiO$_2$ HNs except that 0.65 g TEOS was used as silica precursor.

In a controlled experiment, SiO$_2$ HNs were obtained via calcination of the samples PS@SiO$_2$ HNs under air. **MODIFICATION OF PS/2.5PMA-SIO$_2$ HNS WITH OCTYL GROUP**

PS/2.5PMA-C8-SiO$_2$ CSNs was synthesized by dispersing PS/2.5PMA-SiO$_2$ CSNs in 100 mL n-hexane containing 8 mmol of octyltriethoxysilane and the mixture was refluxed at 70 °C for 24 hours. Then the solid products were isolated and dried at 60 °C overnight. The following ethanol-HCl extraction and THF treatment process was almost the same as PS/2.5PMA-SiO$_2$ HNs. Finally PS/2.5PMA-C8-SiO$_2$ HNs was obtained.

SULFONATION OF PS/nPMA-SIO$_2$ HNS, PS/SIO$_2$ HNS, PS/2.5PMA-C8-SIO$_2$ HNS AND SIO$_2$ HNS

1 g of hybrid HNs were outgassed at 120 °C under vacuum in a two-necked round flask for 3 hours. Then 50 mL of CH$_2$Cl$_2$ containing 10 mL of chlorosulfonic acid was added into the flask at 0 °C. The solution was stirred for 12 hours under argon

2 | *J. Mater. Chem. A*, 2014, **00**, 1-3

This journal is © The Royal Society of Chemistry 2014

atmosphere. The suspension was washed with copious amount of water until the filtrate was neutral. After centrifugation and washing with ethanol, the powder products were dried at 60 ^{o}C overnight. The resulting powder products were denoted accordingly as PS-SO$_3$H/nPMA-SiO$_2$ HNs, PS-SO$_3$H/SiO$_2$ HNs and PS-SO$_3$H/2.5PMA-C8-SiO$_2$ HNs by using PS/nPMA-SiO$_2$ HNs, PS/SiO$_2$ HNs and PS/2.5PMA-C8-SiO$_2$ HNs as precursor, respectively.

ESTERIFICATION OF FATTY ACID WITH ETHANOL

The esterification of lauric acid with ethanol was carried out in a two-necked round flask equipped with a reflux condenser and a magnetic stirrer. The catalyst was pretreated at 120 ^{o}C under vacuum for 3 hours. In a typical run, 5 mL of ethanol and 2 mmol of lauric acid were added to the flask containing 0.05 g of catalyst. The mixture was stirred at 80 ^{o}C and the aliquot was withdrawn by a syringe in regular intervals and analyzed using a precalibrated gas chromatograph (Agilent 6890) equipped with an FID detector and PEG capillary column (30 m × 0.25 mm × 0.25 um). Tetradecane was used as internal standard.

To recycle the solid acid catalyst, the catalyst was filtered from the reaction system, thoroughly washed with ethanol, dried under vacuum at 60 ^{o}C overnight, and directly used in the next cycle.

Characterization

The nitrogen sorption experiments were performed at 77 K using a Micromeritrics ASAP 2020. Samples were degassed at 120 ^{o}C for 6 hours prior to the measurements. The BET surface area was calculated from the adsorption data in the relative pressure P/P$_0$ range from 0.04 to 0.2. Pore size distributions were determined from the adsorption branches using the Barret-Joyner-Halenda (BJH) method. Pore volume was estimated at the relative pressure P/P$_0$ of 0.99. Transmission electron microscopy (TEM) was performed on HITACHI 7700 at an acceleration voltage of 100 kV. High resolution transmission electron microscope (HR-TEM) was performed on a FEI Tecnai G2 F30 S-Twin at an acceleration voltage of 300 kV. Before the measurement, the sample was dispersed in ethanol and deposited on a holey carbon film on a Cu grid. SEM was undertaken by using a FEI Quanta 200F scanning electron microscope operating at an accelerating voltage of 1-30 kV. High-resolution scanning electron microscopy (HR-SEM) was undertaken on a HITACHI S-4800 scanning electron microscope operating at an accelerating voltage of 1-20 kV. FT-IR spectra were collected with a Nicolet Nexus 470 IR spectrometer (KBr pellets were prepared) in the range of 400-4000 cm^{-1}. S elemental analyses were determined by means of an Elementary Vario EL III analyzer. The MAS ^{13}C NMR spectra were recorded on Bruker DRX-400. The experimental parameters are as follows: 8 kHz spin rate, 3 s pulse delay, 4 min contact time, and 1000 scans. Acidic property of the solid materials was monitored by reference to the ^{31}P NMR chemical shift of triethylphosphine oxide (TEPO) chemically adsorbed on the solid acid catalysts. ^{31}P NMR spectra were performed on a Bruker Avance III 600 spectrometer operating at a frequency

of 242.9 MHz using a 4 mm MAS probe. ^{31}P MAS NMR spectra were recorded using high-power proton decoupling with a spinning rate of 12 kHz. 100 scans were accumulated with a π/4 pulse width of 2.25 μs and a 30 s recycle delay. The chemical shifts spectra were referenced to a 85 wt% phosphoric acid external standard. X-ray photoelectron spectroscopy (XPS) measurements were performed on a VG ESCALAB MK2 system, using aluminium Kα X-ray source at 250 W and 12.5 kV. The thermo-gravimetric analysis (TGA) was performed using a NETZSCH STA 449F3 analyzer from 30 ^{o}C to 900 ^{o}C at a heating rate of 10 ^{o}C /min under air atmosphere. The adsorption of water and benzene vapors was measured at 273 K on a Hiden Isochema Intelligent Gravimetric Analyzer after the sample was degassed for 6 h at 393 K. The ultrapure water and benzene used in the vapor adsorption experiments were both treated by freeze-pump-thaw technique for three cycles prior to the adsorption.

The acid exchange capacity of the catalysts was determined by acid-base titration with standard NaOH solution. In a typical procedure, 0.05 g of solid was degassed at 120 ^{o}C for 3 hours and then the sample was suspended in 25 ml of 2 M aqueous NaCl solution. The resulting suspension was stirred at room temperature for 24 hours until equilibrium was reached, and subsequently titrated with standard NaOH solution.

Results and discussion

Synthesis of PS/nPMA-SiO$_2$ HNs and PS-SO$_3$H/nPMA-SiO$_2$ HNs
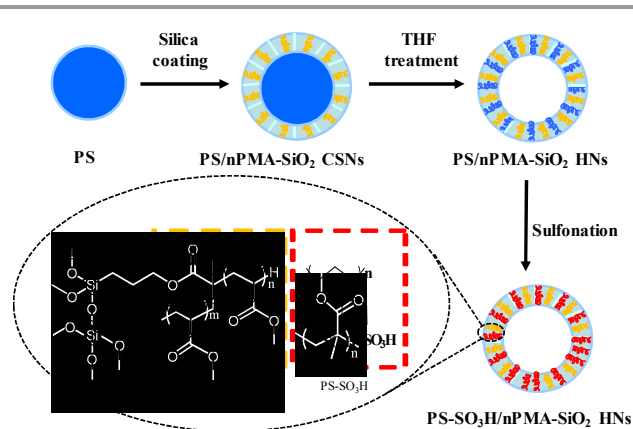
Scheme 1 General procedure for the synthesis of mesoporous silica HNs with uniform distribution of PMA and sulfonated PS

PS-SO$_3$H/nPMA-SiO$_2$ HNs were obtained by sulfonation of PS/nPMA-SiO$_2$ HNs with chlorosulfonic acid (Scheme 1). Polymer nanospheres, such as polystyrene (PS), poly(methyl methacrylat) (PMMA) ect., have been widely used as hard templates for the synthesis of hollow nanospheres[43-47]. After hard template removing either by calcination or extracting method, the hollow nanostructure was generated. In our previous report[41], it was found that the dissolved PMMA chains could be kept in the mesochannels of silica shells for the formation of hybrid silica HNs with high concentration of

This journal is © The Royal Society of Chemistry 2014

J. Mater. Chem. A., 2014, **00**, 1-3 | **3**

PMMA based on the ''dissolution and entrapment'' strategy which was proposed for the first time. Specially the functional group PMA (poly(methacrylate) which is incorporated into the mesoporous SiO_2 shell can efficiently entrap the dissolved PMMA. Here the similar strategy was employed for the synthesis of PS/nPMA-SiO$_2$ HNs (Scheme 1). In the first step, PS nanospheres were coated with a mixture of TEOS and PMA-Si using CTAB as mesostructure directing agent according to a modified stöber method[48]. During the sol-gel process, the hydrolysis and polymerization of TEOS and PMA-Si formed a hybrid mesoporous shell on the PS template nanospheres and PS/nPMA-SiO$_2$ core shell nanospheres (CSNs) were obtained (Figures 1 and S1). After THF treatment, PS/nPMA-SiO$_2$ HNs were obtained. The successful transformation from core shell to hollow nanospheres after THF treatment is shown in Figure 1, taken PS/5PMA-SiO$_2$ HNs as a representative. It should be mentioned that the particle size of PS/5PMA-SiO$_2$ HNs remains unchanged after THF treatment, exhibiting that the dissolved PS is mainly distributed in the mesopore of the shell. The above result clearly suggests that the dissolution of PS cores during the THF extraction process is the main driving force for the formation of hollowed structure. The loading of PS could be facilely tuned by varying the ratio of PS to silica percrsor during the silica coating process.
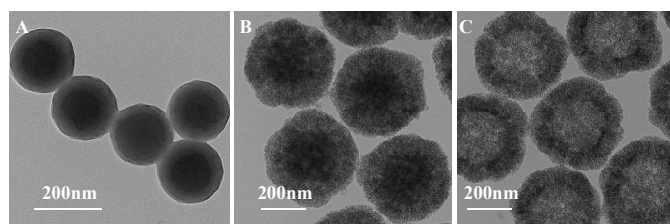

Figure 1 TEM images of PS template nanospheres (A), PS/5PMA-SiO$_2$ CSNs (B) and PS/5MA-SiO$_2$ HNs (C)

As a control sample, PS/SiO$_2$ HNs without PMA-Si incorporated in the shell, were prepared in a similar way to PS/5PMA-SiO$_2$ HNs. The results of thermo gravimetric (TG) show that weight loss for PS/SiO$_2$ HNs and PS/5PMA-SiO$_2$ HNs before and after THF treatment is 10% and 3.65 wt%, respectively (Figure S2). These results indicated that the PMA-Si incorporated into the mesoporous shell can efficiently entrap the dissolved PS in the mesoporous shell. The sulfonation of PS/5PMA-SiO$_2$ HNs and PS/SiO$_2$ HNs straightforwardly results in the formation of hybrid solid acids.

Characterization of PS/nPMA-SiO$_2$ HNs

The TEM images of PS/nPMA-SiO$_2$ HNs and PS/SiO$_2$ HNs are shown in Figure 2. The TEM images show that all samples are monodispersed hollow nanospheres and the particle size increases as the ratio of PMA-Si silane precursor to PS increases. The particle size increased from about 340 nm to 400 nm as the n increase from 2.5 to 5. Accordingly, the thickness of the hybrid silica shells also increased from 50 nm to 80 nm. This is reasonable because more siliane precursors are used as

the n increases. Based on the TEM image, PS/nPMA-SiO$_2$ HNs and PS/SiO$_2$ HNs all have the mesoporous channels aligning perpendicular to the cores, which would benefit the diffusion of reactants and products during the catalytic process. Compared with PS/SiO$_2$ HNs, PS/nPMA-SiO$_2$ HNs have larger mesopore and less condensed shell. For surface modification, PS/2.5PMA-SiO$_2$ HNs was grafted with octyl for the generation PS/2.5PMA-C8-SiO$_2$ HNs. PS/2.5PMA-C8-SiO$_2$ HNs have the same morphology as the parent PS/2.5PMA-SiO$_2$ HNs based in the TEM characterization, showing the grafting process does not damage the nanostructure and morphology of the hybrid HNs (Figure 2).
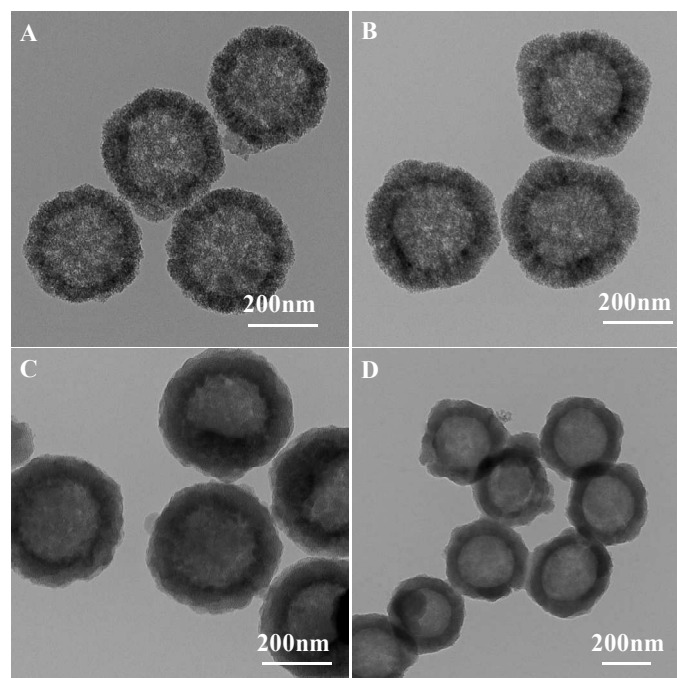

Figure 2 TEM images of PS/2.5PMA-SiO$_2$ HNs (A), PS/3.3PMA-SiO$_2$ HNs (B), PS/SiO$_2$ HNs (C) and PS/2.5PMA-C8-SiO$_2$ HNs (D)

The textural properties of the obtained hybrid hollow nanospheres were investigated by nitrogen adsorption-desorption at 77 K. Figures 3A and 3B show the N$_2$ adsorption-desorption isotherms and corresponding pore size distribution of PS/SiO$_2$ HNs and PS/nPMA-SiO$_2$ HNs, respectively. The adsorption-desorption isotherms of the samples display type-IV isotherm patterns which is typical for mesoporous silica synthesized with CTAB as a surfactant[40]. PS/SiO$_2$ HNs exhibits sharp capillary condensation step at P/P$_0$ less than 0.3, while PS/nPMA-SiO$_2$ HNs shows H4-type hysteresis loop starting from the relative pressure P/P$_0$ at 0.45, indicating that PS/nPMA-SiO$_2$ HNs have larger mesopore than PS/SiO$_2$ HNs. This is also verified by the pore size distribution curves and consistent with the TEM results. The pore size distribution curves also show that PS/SiO$_2$ HNs have more uniform distribution of mesopore than PS/nPMA-SiO$_2$ HNs, probably due to the interruption of PMA polymer chain on the mesostructure formation. The textural parameters of PS/SiO$_2$ HNs and PS/nPMA-SiO$_2$ HNs are summarized in Table 1. The

4 | J. Mater. Chem. A., 2014, 00, 1-3

This journal is © The Royal Society of Chemistry 2014

BET surface area of PS/SiO$_2$ HNs and PS/nPMA-SiO2 HNs varies in the range of 89 to 297 m^{2}g^{-1} and pore volume varies in the range of 0.14 to 0.26 cm^{3}g^{-1}. Compared with PS/2.5PMA-SiO$_2$ HNs, only slight decrease in the BET surface area was observed for PS/2.5PMA-C8-SiO$_2$ HNs.
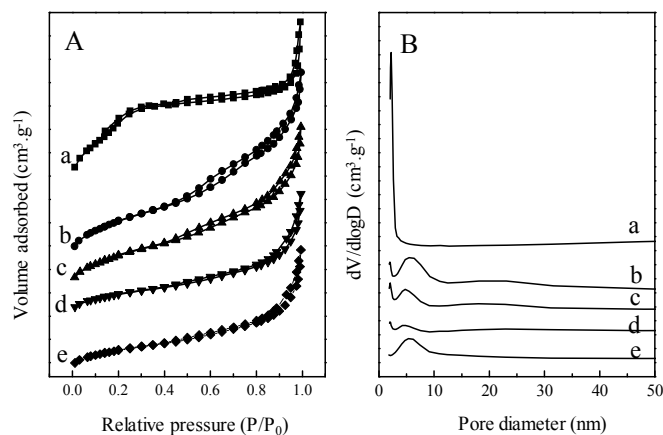

Figure 3 N$_2$ adsorption-desorption isotherms (**A**) and the pore size distribution curves of PS/SiO$_2$ HNs (**a**), PS/5PMA-SiO$_2$ HNs (**b**), PS/3.3PMA-SiO$_2$ HNs (**c**), PS/2.5PMA-SiO$_2$ HNs (**d**) and PS/2.5PMA-C8-SiO$_2$ HNs (**e**)

Table 1. The textural parameters and polymer content of PS/nPMA-SiO$_2$ HNs and PS/SiO$_2$ HNs before and after sulfonation^a

Samples	S$_{BET}$ (m^{2}g^{-1})	D^b_p (nm)	V$_p$ (cm^{3}g^{-1})	Polymer content^c (wt. %)
PS/SiO$_2$ HNs	297 (331)	2.2 (2.5)	0.19 (0.30)	32.5
PS/5PMA-SiO$_2$	180 (149)	5.5 (6.4)	0.26 (0.21)	64.2
PS/3.3PMA-SiO$_2$	153 (164)	4.4 (4.8)	0.21 (0.21)	66.4
PS/2.5PMA-SiO$_2$	89 (128)	5.4 (4.4)	0.14 (0.14)	68.2
PS/2.5PMA-C8-SiO$_2$	88 (115)	5.8 (4.2)	0.12 (0.13)	72
Amberlyst®-15	(45)	(40)	(0.31)	-

^{a} Data in the parenthesis is for the samples after sulfonation; ^{b}Pore size distribution estimated from BJH model; ^{c} Polymer content estimated based on TG results.

Based on the TG analysis, the polymer content was calculated by the weight loss in the range of 200-700 °C (Table 1 and Figure S3). The weight loss of PS/SiO$_2$ HNs in the temperature range of 200-700 °C is 32.5 %. For the PS/nPMA-SiO$_2$ HNs, much higher polymer content was obtained because of introducing of the PMA polymer. PS/5PMA-SiO$_2$ HNs affords the weight loss of 64.2 %. From PS/5PMA-SiO$_2$ HNs to PS/2.5PMA-SiO$_2$ HNs, only about 5.3 % increase in weight

loss was observed, indicating that polymer/silica weight ratio has the upper limit in the hybrid HNs. The above results show that PS/nPMA-SiO$_2$ HNs with high content PS and PMA have been successfully synthesized. The weight loss of PS/2.5PMA-C8-SiO$_2$ HNs is about 3.8 % higher than PS/2.5PMA-SiO$_2$ HNs based on the TG results (Figure S4).

Characterization of PS-SO$_3$H/nPMA-SiO$_2$ HNs

PS-SO$_3$H/SiO$_2$ HNs, PS-SO$_3$H/nPMA-SiO$_2$ HNs and PS-SO$_3$H/2.5PMA-C8-SiO$_2$ HNs were obtained by direct sulfonation of the corresponding hybrid HNs with ClSO$_3$H in CH$_2$Cl$_2$ at 0 °C for 12 hours. The TEM images of sulfonated hybrid HNs are shown in Figure 4. PS-SO$_3$H/SiO$_2$ HNs, PS-SO$_3$H/nPMA-SiO$_2$ HNs and PS-SO$_3$H/2.5PMA-C8-SiO$_2$ HNs have uniform hollow nanostructure with almost the same particle size and shell thickness to the parent hybrid HNs, indicting the stability of the hybrid HNs in strongly acid media. Taken PS-SO$_3$H/SiO$_2$ for example the SEM image (Figure 4F) clearly shows the sample after sulfonation has similar nanospherical morphology as that before sulfonation. The HR-SEM images shown in Figure S5 further verify that all sulfonated hybrid HNs is composed of uniform and mono-dispersed nanospheres with porous rough surface.
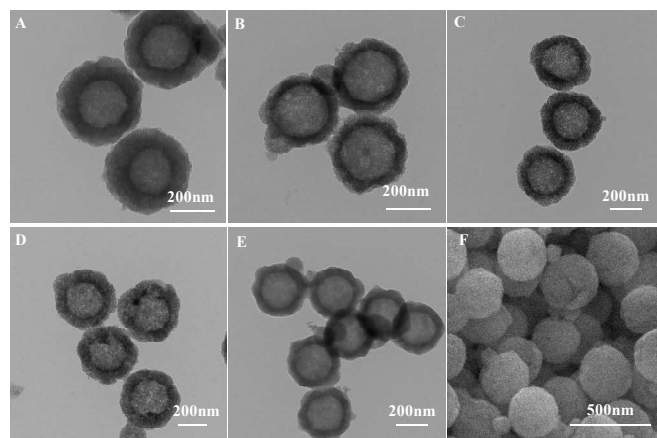

Figure 4 TEM images of PS-SO$_3$H/SiO$_2$ HNs (**A**), PS-SO$_3$H/2.5PMA-SiO$_2$ HNs (**B**), PS-SO$_3$H/3.3PMA-SiO$_2$ HNs (**C**), PS-SO$_3$H/5PMA-SiO$_2$ HNs (**D**), PS-SO$_3$H/5PMA-C8-SiO$_2$ HNs (**E**) and SEM image of PS-SO$_3$H/SiO$_2$ HNs (**F**)

The successful sulfonation of PS in the hybrid nanospheres was verified by FT-IR, XPS and ^{13}C NMR spectroscopy (Figure 5, Figure S6 and Figure S7). In the FT-IR spectra (Figure S6) the appearances of characteristic vibration of PMA at 1740 cm^{-1} arises from a C=O stretching vibration[41, 42] suggested the successful incorporation of the PMA polymer fragment into the mesoporous network of PS/nPMA-SiO$_2$ HNs as well as PS-SO$_3$H/nPMA-SiO$_2$ HNs. The new peaks attributed to sulfonic acid groups at 581, 1011 and 1415 cm^{-1} appeared in the FT-IR spectra of PS-SO$_3$H/SiO$_2$ HNs and PS-SO$_3$H/nPMA-SiO$_2$, while the intensity of C-H deformation vibration of monosubstituted phenyl groups at 700-750 cm^{-1} decreases apparently. In the XPS spectra (Figure 5A) the S 2p peak at 173.2 eV was observed, confirming the incorporation of sulfonic acid groups. ^{13}C NMR spectrum of PS-SO$_3$H/SiO$_2$

HNs clearly show the signal at around 142 ppm which could be assigned to the aromatic carbon coordinated with sulfonic acid groups. These results imply a successful sulfonation of PS with the current sulfonation method (Figure S7).
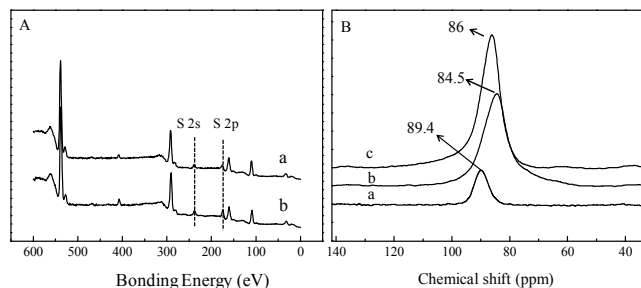

Figure 5. XPS spectra (**A**)of PS-SO$_3$H/SiO$_2$ HNs (**a**) and PS-SO$_3$H/5PMA-SiO$_2$ HNs (**b**); (**B**) ^{31}P MAS NMR spectra of Amberlyst®-15 (**a**)[49], PS-SO$_3$H/SiO$_2$ HNs (**b**) and PS-SO$_3$H/5PMA-SiO$_2$ HNs (**c**)

The acid strength of Amberlyst®-15, PS-SO$_3$H/SiO$_2$ HNs and PS-SO$_3$H/5PMA-SiO$_2$ HNs was investigated using TEPO (triethylphosphine oxide) as a probe molecule in combination with ^{31}P MAS NMR technique (Figure 5 B). The ^{31}P chemical shift of TEPO chemisorbed on the acid site is sensitive to acid strength, and stronger acid strength will usually lead to larger ^{31}P chemical shift of TEPO. The ^{31}P NMR spectrum of Amberlyst ® -15 exhibits a signal at 89.4 ppm which was assigned to TEPO adsorbed on SO$_3$H acid sites[49]. PS-SO$_3$H/SiO$_2$ HNs and PS-SO$_3$H/5PMA-SiO$_2$ HNs exhibit a signal at 84.5 ppm and 86 ppm respectively. The lower chemical shift indicates PS-SO$_3$H/SiO$_2$ HNs and PS-SO$_3$H/5PMA-SiO$_2$ HNs have the weaker acid strength than Amberlyst®-15. However PS-SO$_3$H/5PMA-SiO$_2$ HNs exhibit larger chemical shift than PS-SO$_3$H/SiO$_2$ HNs indicating the incorporation of PMA polymer could help to enhance the acid strength.

For further illustrating the distribution of sulfonic acid groups in the mesoporous shells of PS-SO$_3$H/nPMA-SiO$_2$ HNs, the HR-TEM element mapping analysis was used as the direct evidence for the location of sulfur (Figure 6). The HR-TEM element mapping images clearly show that the Si and S element was distributed uniformly in the outer shells of the hollow nanospheres. The sulfonic acid groups located uniformly in the outer shells may favor the access of reactants to active sites during the catalytic process.
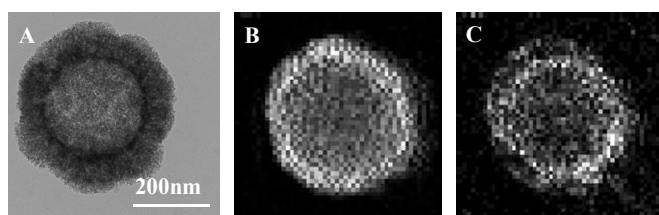

Figure 6 TEM images of PS-SO$_3$H/5PMA-SiO$_2$ HNs (**A**) and EDS mapping analysis of Si element (**B**) and S element (**C**) according to TEM image shown in **A**

PS/SiO$_2$ HNs display a sharp diffraction peak at low diffraction angle, showing the sample has ordered mesoporous structure. A broad diffraction peak was observed in the XRD pattern of PS/5PMA-SiO$_2$ HNs. This suggests that the incorporation of PMA polymer causes the deterioration of the mesostructure. PS-SO$_3$H/5PMA-SiO$_2$ HNs has similar XRD pattern to that of PS/5PMA-SiO$_2$ HNs, confirming that the sulfonation process does not cause the destruction of the mesoporous structure (Figure S8).
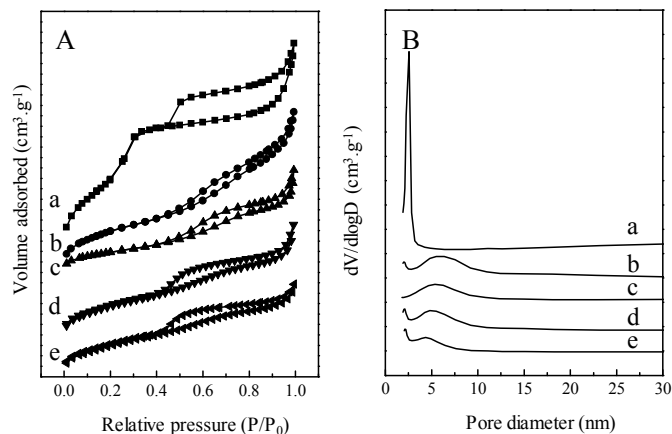

Figure 7 N$_2$ adsorption-desorption isotherms (A) and the corresponding pore size distribution of PS-SO$_3$H/SiO$_2$ HNs (**a**), PS-SO$_3$H/5PMA-SiO$_2$ HNs (**b**), PS-SO$_3$H/3.3 PMA-SiO$_2$ HNs (**c**), PS-SO$_3$H/2.5PMA-SiO$_2$ HNs (**d**) and PS-SO$_3$H/2.5PMA-C8-SiO$_2$ HNs (**e**)

The sulfonated hybrid HNs exhibit type-IV isotherm patterns similar to the parent materials (Figure 7). It should be mentioned that an obvious H4 hysteresis loop appears in the N$_2$ isotherm of PS-SO$_3$H/SiO$_2$ HNs, which is probably due to the existence of defects caused during the sulfonation process. The textural parameters of the sulfonated hybrid HNs are summarized in Table 1. Only slight decrease in BET surface area was observed after sulfonation. The BET surface area of the sulfonated hybrid varies in the range of 331 to 115 m^{2}g^{-1} which were much higher than that of Amberlyst®-15.

In order to quantitatively analyze the amount of active sites of the sulfonated hybrid HNs, the sulfur content and acid exchange capacity were obtained by element analysis and acid-base titration method respectively (Table 2). Increasing the amount of PMA in the hybrid HNs results in the decreasing of the acid exchange capacity and sulfur content while higher content of PS in the hybrid HNs benefits high content of acid sites. The acid exchange capacity of the sulfonated hybrid HNs varies from 0.90 to 2.0 mmolg^{-1} while the sulfur content varies from 0.99 to 2.2 mmolg^{-1}. For the PS-SO$_3$H/nPMA-SiO$_2$ HNs samples, the acid exchange capacity and the sulfur content was very similar. However for PS-SO$_3$H/SiO$_2$ HNs the sulfur content were higher than the acid exchange capacity. The H-bond interactions may exist among sulfonic acid groups and hydroxyl groups in the mesoporous shells for PS-SO$_3$H/SiO$_2$ HNs, which may reduce the accessibility of acid sites during the titration process. For the PS-SO$_3$H/nPMA-SiO$_2$ HNs samples the incorporation of the polymer PMA may help to weaken the interactions among sulfonic acid groups and silicon

6 | *J. Mater. Chem. A*., 2014, **00**, 1-3

This journal is © The Royal Society of Chemistry 2014

hydroxyl groups. Thus the acid exchange capacity is similar to the sulfur content. Based on the results we can see that the acid exchange capacity and the sulfur element content were consistent and this consistence between H^+ and sulfur suggests that all of the acid sites were available during the titration process.

Catalytic performance of hybrid mesoporous silica hollow nanospheres

Esterification of fatty acid with ethanol was chosen as the model reaction for investigating the catalytic performance of the sulfonated hybrid HNs (Table 2). The esterification of fatty acids with alcohol to produce esters represents an important pretreatment step in the production of biodiesel from high free fatty acid feed stocks. Firstly a controlled blank experiment was carried out for the esterification of lauric acid with ethanol and only 1.5% yield of laurate ethyl was obtained. For the sulfonated SiO_2 HNs samples only 4.9% yield of laurate ethyl was obtained indicating the sulfonic acid groups functionalized surface silanol groups using the same method could be negligible. Under similar reaction conditions, all sulfonated hybrid HNs could efficiently catalyze the reaction, showing that the sulfonic acid groups are the active sites for this reaction. The catalytic performance of the concentrated sulfuric acid and commercially available Amberlyst®-15 was also investigated. Among all samples, the concentrated sulfuric acid affords the highest reaction rate (TOF of 29.3±0.1 h^{-1}) as expected and Amberlyst®-15 gives the lowest reaction rate with TOF of 2.4±0.1 h^{-1}. The low activity of Amberlyst®-15 is mainly due to its low surface area. The TOF of the sulfonated hybrid HNs varies in the range of 27.3±0.3 to 16.3±0.1 h^{-1}. The relatively high activity of PS-SO_3H/5PMA-SiO_2 HNs and PS-SO_3H/SiO_2 HNs in comparison with Amberlyst®-15 suggests that PS-SO_3H is uniformly algined in the mesoporous silica shell may benefit to increase the accessibility of reactants to the sulfonic acid groups and the mesoporous shell would facilitate the fast diffusion of reactants and products during the catalytic process.

SO_3H/5PMA-SiO_2 HNs with TOF of 27.3±0.3 h^{-1} is almost as active as H_2SO_4.

Though PS-SO_3H/SiO_2 HNs have higher BET surface area and acid exchange capacity than PS-SO_3H/nPMA-SiO_2 HNs, PS-SO_3H/nPMA-SiO_2 HNs are more active than PS-SO_3H/SiO_2. It has been reported that PMA is a hydrophobic polymer and its incorporation may modify the surface properties of the hybrid HNs[42]. So water/oil adsorption experiments were performed to investigate the surface hydrophobicity. As reported[38, 50, 51], the water and benzene adsorption capacities at the low relative pressure range ($P/P_0 \leqslant 0.30$) were used for the calculation (Table 2). The results show that adsorbed benzene/water molar ratio for PS-SO_3H/nPMA-SiO_2 HNs is higher than that for PS-SO_3H/SiO_2 HNs, showing that PS-SO_3H/nPMA-SiO_2 HNs have more hydrophobic surface properties than PS-SO_3H/SiO_2 HNs. So the low activity of PS-SO_3H/SiO_2 nanocomposites is attributed to its more hydrophilic surface properties and also the smaller pore size. The octyl modification could further increase the surface hydrophobicity[52]. PS-SO_3H/2.5PMA-C8-SiO_2 HNs with octyl group incorporation shows the higher activity than PS-SO_3H/2.5PMA-SiO_2 HNs (19.1±0.1 versus 16.3±0.1 h^{-1}) (BET surface area and pore volume were almost the same for the two samples). In combination with the catalytic results, it could be suggested that hydrophobic surface is more favorable for obtaining higher catalytic activity. Previous studies suggest that hydrophobicity of the solid catalysts could increase the catalytic activity due to protective effect of acid sites from water attacking, the increased diffusion rate of the hydrophobic reactants and high enrichment effect for the reactants[5, 52, 53]. For PS-SO_3H/nPMA-SiO_2 HNS, the TOF decreases monotonically with the increase in the surface hydrophobicity. This is due to decrease in the BET surface area because the textural properties also affect the catalytic activity of the solid materials in addition to the surface properties.

The catalytic stability of the sulfonated hybrid HNs was tested using PS-SO_3H/2.5PMA-SiO_2 HNs and PS-SO_3H/2.5PMA-C8-SiO_2 HNs as model catalysts in the esterification of lauric acid

Table 2. The sulfur content, acid exchange capacity and surface properties of sulfonated hybrid HNs and their catalytic performance in the esterification of lauric acid with ethanol.

Sample	S content[a] (mmolg^{-1})	H^+content[b] (mmolg^{-1})	Adsorbed benzene/water molar ratio	TOF (h^{-1})	Conv. (%)
H_2SO_4	-	-	-	29.3±0.1	93.7±1.7
Amberlyst®-15	-	4.7	-	2.4±0.1	65.3±0.8
PS-SO_3H/SiO_2 HNs	2.29	2.0	0.08	13.6±0.3	87.8±0.1
PS-SO_3H/5PMA-SiO_2	0.99	0.9	0.11	27.3±0.2	88.9±0.6
PS-SO_3H/3.3PMA-SiO_2	1.43	1.5	0.12	21.1±0.2	91.6±0.2
PS-SO_3H/2.5PMA-SiO_2	1.80	1.9	0.24	16.3±0.1	91.6±0.6
PS-SO_3H/2.5PMA-C8-SiO_2	1.79	1.8	0.27	19.1±0.1	94.7±0.1
SiO_2 HNs	-	-	-	-	4.9

[a] Measured by element analysis; [b] Measured by acid-base titration method.

Actually, most solid acid catalysts reported exhibit much lower activity than H_2SO_4. It should be mentioned that PS-

with ethanol (Figure 8). For the second cycle, the yield of ethyl lauric over PS-SO_3H/2.5PMA-SiO_2 HNs decreases sharply from 96.3% to 71.1%. For the next several cycles, the

This journal is © The Royal Society of Chemistry 2014

J. Mater. Chem. A., 2014, **00**, 1-3 | 7

conversion only slightly decreases. After ten cycles, the conversion is about half of the first cycle. The acid exchange capacity of PS-SO$_3$H/2.5PMA-SiO$_2$ HNs after 10 cycles was 1.0 mmol/g, only half of the fresh catalyst. This shows that the leaching of active sites is the main reason for the deactivation of the hybrid HNs. However for PS-SO$_3$H/2.5PMA-C8-SiO$_2$ HNs after 10 cycle, the conversion only decreases from 96.3 to 79.6 % and the activity of the catalyst could still retain 82% of the fresh one. The acid exchange capacity of PS-SO$_3$H/2.5PMA-C8-SiO$_2$ HNs after 10 cycles is 1.8 mmolg^{-1}, only slightly decreases in comparison with the fresh one (1.9 mmolg^{-1}). The above results suggest that PS-SO$_3$H/2.5PMA-C8-SiO$_2$ HNs with octyl group modification are much more stable than PS-SO$_3$H/2.5PMA-SiO$_2$ HNs without octyl modification, suggesting that octyl group could efficiently prevent the leaching of active sites during the catalytic process. We guess that the hydrophobic carbon chain may tangle with the sulfonated PS polymer chain to increase its stability during the catalytic process.
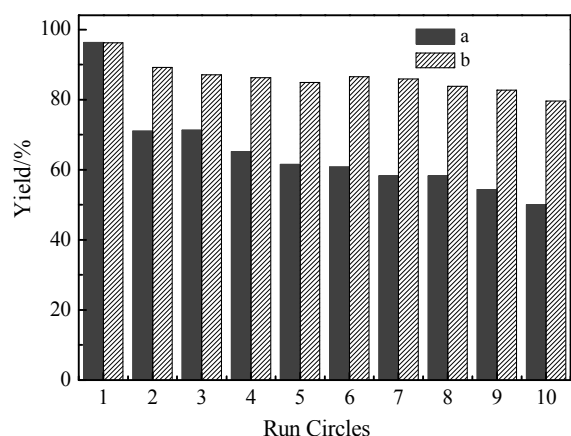

Figure 8 Catalytic recycle stability of PS-SO$_3$H/2.5PMA-SiO$_2$ HNs (a) and PS-SO$_3$H/2.5 PMA-C8-SiO$_2$ HNs (b) in the esterification of lauric acid with ethanol

Conclusions

In summary, we have demonstrated an efficient strategy for the synthesis of hybrid hollow nanospheres with high content of sulfonic groups uniformly distributed in mesoporous silica channels. The hybrid HNs have a BET surface area from 115 to 331 m^{2}g^{-1} and pore size from 2.5 nm to 6.4 nm, depending on the polymer content incorporated in the silica shell. The hybrid HNs could be used as efficient solid acid catalysts for acid-catalyzed liquid reactions such as esterification of lauric with ethanol. The studies show that the incorporation of PMA and surface modification by octyl group could increase the surface hydrophobicity, which causes an increase in the catalytic activity. Under similar conditions, the hybrid HNs with optimized surface properties and sufonic acid content show comparable activity to the concentrated sulfuric acid. The incorporated octyl group could prevent the leaching of PS-SO$_3$H during the catalytic process, thus, the hybrid HNs could be stably recycled. Our results provide a new approach for the synthesis of solid acid catalysts by efficiently combining PS-SO$_3$H and silica and hollow nanostructure together.

Notes and references

^{a} State Key Laboratory of Catalysis, Dalian Institute of Chemical Physics, Chinese Academy of Sciences, 457 Zhongshan Road, Dalian 116023, China. E-mail: yangqh@dicp.ac.cn; Web: http://www.hmm.dicp.ac.cn; Tel: 86-411-84379552. Fax: 86-411-84694447.
^{b} University of Chinese Academy of Sciences, Beijing 100049, China.

† Electronic Supplementary Information (ESI) available: [details of any supplementary information available should be included here]. See DOI: 10.1039/b000000x/

1. A. Corma, Chem. Rev., 1995, **95**, 559.
2. J. H. Clark, Acc. Chem. Res., 2002, **35**, 791.
3. G. Busca, Chem. Rev., 2007, **107**, 5366.
4. F. Liu, X. Meng, Y. Zhang, L. Ren, F. Nawaz and F. Xiao, J. Catal., 2010, **271**, 52.
5. F. Liu, W. Kong, C. Qi, L. Zhu and F. Xiao, Acs Catal., 2012, **2**, 565.
6. R. Xing, N. Liu, Y. Liu, H. Wu, Y. Jiang, L. Chen, M. He and P. Wu, Adv. Funct. Mater., 2007, **17**, 2455.
7. P. A. Zapata, J. Faria, M. P. Ruiz, R. E. Jentoft and D. E. Resasco, J. Am. Chem. Soc., 2012, **134**, 8570.
8. F. Bauer, W. H. Chen, E. Biiz, A. Freyer, V. Sauerland and S. Liu, J. Catal., 2007, **251**, 258.
9. M. Tamura, W. Chaikittisilp, T. Yokoi and T. Okubo, Microporous Mesoporous Mater., 2008, **112**, 202.
10. C. Tagusagawa, A. Takagaki, S. Hayashi and K. Domen, J. Am. Chem. Soc., 2008, **130**, 7230.
11. J. B. Joo, A. Vu, Q. Zhang, M. Dahl, M. Gu, F. Zaera and Y. Yin, ChemSusChem, 2013, **6**, 2001.
12. G. D. Yadav and J. J. Nair, Microporous Mesoporous Mater., 1999, **33**, 1.
13. Y. Xu, W. Gu and D. Gin, J. Am. Chem. Soc., 2004, **126**, 1616.
14. M. A. Harmer, W. E. Farneth and Q. Sun, J. Am. Chem. Soc., 1996, **118**, 7708.
15. P. R. Siril, H. E. Cross and D. R. Brown, J. Mol. Catal. A: Chem., 2008, **279**, 63.
16. M. A. Harmer and Q. Sun, Appl. Catal. A, 2001, **221**, 45.
17. M. Hart, G. Fuller, D. R. Brown, J. Mol. Catal. A: Chem., 2002, **182**, 439.
18. P. Barbaro and F. Liguori, Chem. Rev., 2009, **109**, 515.
19. C. T. Kresge and W. J. Roth, Chem. Soc. Rev., 2013, **42**, 3663.
20. S. Shylesh, P. P. Samuel, S. Sisodiya and A. P. Singh, Catalysis Surveys from Asia, 2008, **12**, 266.
21. F. Hoffmann, M. Cornelius, J. Morell and M. Froeba, Angew. Chem. Int. Ed., 2006, **45**, 3216.
22. A. Sayari and S. Hamoudi, Chem. Mater., 2001, **13**, 3151.
23. L. Zhang, Q. Yang, W. Zhang, Y. Li, J. Yang, D. Jiang, G. Zhu and C. Li, J. Mater. Chem., 2005, **15**, 2562.
24. Y. Yang, J. Liu, X. Li, X. Liu and Q. Yang, Chem. Mater., 2011, **23**, 3676.

8 | *J. Mater. Chem. A*, 2014, **00**, 1-3

This journal is © The Royal Society of Chemistry 2014

25. Y. Yang, X. Liu, X. Li, J. Zhao, S. Bai, J. Liu and Q. Yang, Angew. Chem. Int. Ed., 2012, **51**, 9164.

26. X. Li, X. Liu, Y. Ma, M. Li, J. Zhao, H. Xin, L. Zhang, Y. Yang, C. Li and Q. Yang, Adv. Mater., 2012, **24**, 1424.

27. J. Liu, Q. Yang, L. Zhang, H. Yang, J. Gao and C. Li, Chem. Mater., 2008, **20**, 4268.

28. W. Long and C. W. Jones, Acs Catal., 2011, **1**, 674.

29. D. Margolese, J. A. Melero, S. C. Christiansen, B. F. Chmelka and G. D. Stucky, Chem. Mater., 2000, **12**, 2448.

30. J. A. Melero, G. D. Stucky, R. van Grieken and G. Morales, J. Mater. Chem., 2002, **12**, 1664.

31. T. Okayasu, K. Saito, H. Nishide and M. T. W. Hearn, Green Chem., 2010, **12**, 1981.

32. A. Martin, G. Morales, F. Martinez, R. van Grieken, L. Cao and M. Kruk, J. Mater. Chem., 2010, **20**, 8026.

33. M. Choi, F. Kleitz, D. N. Liu, H. Y. Lee, W. S. Ahn and R. Ryoo, J. Am. Chem. Soc., 2005, **127**, 1924.

34. R. E. Mishler, II, A. V. Biradar, C. T. Duncan, E. A. Schiff and T. Asefa, Chem. Commun., 2009, **41**, 6201.

35. H. Chen, R. Liu, M. Lo, S. Chang, L. Tsai, Y. Peng and J. Lee, J. Phys. Chem. C, 2008, **112**, 7522.

36. J. Gao, J. Liu, S. Bai, P. Wang, H. Zhong, Q. Yang and C. Li, J. Mater. Chem., 2009, **19**, 8580.

37. J. Y. Kim, J. C. Park, H. Kang, H. Song and K. H. Park, Chem. Commun., 2010, **46**, 439.

38. P. Wang, S. Bai, J. Zhao, P. Su, Q. Yang and C. Li, ChemSusChem, 2012, **5**, 2390.

39. Z. Feng, Y. Li, D. Niu, L. Li, W. Zhao, H. Chen, L. Li, J. Gao, M. Ruan and J. Shi, Chem. Commun., 2008, **23**, 2629.

40. J. Dou and H. C. Zeng, J. Am. Chem. Soc., 2012, **134**, 16235.

41. L. Zhang, S. Wu, C. Li and Q. Yang, Chem. Commun., 2012, **48**, 4190.

42. J. Liu, J. Peng, S. Shen, Q. Jin, C. Li and Q. Yang, Chem. Eur. J., 2013, **19**, 2711.

43. M. Chen, L. Wu, S. Zhou and B. You, Adv. Mater., 2006, **18**, 801.

44. Z. Deng, M. Chen, S. Zhou, B. You and L. Wu, Langmuir, 2006, **22**, 6403.

45. Z. Zhong, Y. Yin, B. Gates and Y. Xia, Adv. Mater., 2000, **12**, 206.

46. H. Blas, M. Save, P. Pasetto, C. Boissiere, C. Sanchez and B. Charleux, Langmuir, 2008, **24**, 13132.

47. G. Qi, Y. Wang, L. Estevez, A. K. Switzer, X. Duan, X. Yang and E. P. Giannelis, Chem. Mater., 2010, **22**, 2693.

48. W. Stober, A. Fink and E. Bohn, J. Colloid Interface Sci., 1968, **26**, 62.

49. X. Zhang, Y. Zhao, S. Xu, Y. Yang, J. Liu, Y. Wei and Q. Yang, Nat. Commun., 2014, doi:10.1038/ncomms4170.

50. S. Inagaki and Y. Fukushima, Microporous Mesoporous Mater., 1998, **21**, 667.

51. J. Pires, M. Pinto, J. Estella, J. C. Echeverria, J. Colloid Interface Sci., 2008, **317**, 206.

52. J. P. Dacquin, H E. Cross, D. R. Brown, T. Duren, J. J. Williams, A. F. Lee, K. Wilson, Green Chem., 2010, **12**, 1383.

53. K. Inumaru, T. Ishihara, Y. Kamiya, T. Okuhara, S. Yamanaka, Angew. Chem. Int. Ed., 2007, **46**, 7625.